

# The Ubiquity and Magnitude of Large FeK $\alpha$ Equivalent Widths in AGN Extended Regions

P. Tzanavaris,<sup>1,2,3</sup> T. Yaqoob,<sup>1,2</sup> and S. LaMassa<sup>4</sup>

<sup>1</sup>*Center for Space Science and Technology, University of Maryland,  
Baltimore County, 1000 Hilltop Circle, Baltimore, MD 21250*

<sup>2</sup>*Center for Research and Exploration in Space Science and Technology,  
NASA/Goddard Space Flight Center, Greenbelt, MD 20771*

<sup>3</sup>*The American Physical Society, Hauppauge, New York 11788*

<sup>4</sup>*Space Telescope Science Institute, 3700 San Martin Drive, Baltimore, MD 21218*

(Dated: December 4, 2023)

Narrow Fe K $\alpha$  fluorescent emission lines arising at  $\sim$ kpc-scale separations from the nucleus have only been detected in a few AGN. The detections require that the extended line emission be spatially resolved and sufficiently bright. Compared to narrow Fe K $\alpha$  lines arising closer to the nucleus, they have much lower fluxes but show substantially larger equivalent widths,  $EW_{\text{FeK}\alpha}$ . We show that, in the optically-thin limit, a purely analytical argument naturally predicts large,  $EW_{\text{FeK}\alpha} \sim 1$  keV, values for such lines, regardless of the details of equivalent hydrogen column density,  $N_{\text{H}}$ , or reprocessor geometry. Monte Carlo simulations corroborate this result and show that the simple analytic  $EW_{\text{FeK}\alpha}$  prescription holds up to higher  $N_{\text{H}}$  approaching the Compton-thick regime. We compare to *Chandra* observations from the literature and discuss that our results are consistent with the large  $EW_{\text{FeK}\alpha}$  values reported for local AGN, for which the line is detected in extended, up to  $\sim$ kpc-scale, regions. We argue that large  $EW_{\text{FeK}\alpha}$  from kpc-scale regions in AGN should be ubiquitous, because they do not depend on the absolute luminosity of the central X-ray source, and are measured only against the scattered continuum. We predict values to be of the order of  $\sim 1$  keV or larger, even for covering factors  $\ll 1$ , and for arbitrarily small column densities. We propose that the large-scale molecular material that is now routinely being detected with the Atacama Large Millimeter/Submillimeter Array (ALMA) may act as an extended X-ray scattering reprocessor giving rise to  $\sim$ kpc-scale Fe K $\alpha$  emission.

Keywords: black hole physics – radiation mechanisms: general – scattering – galaxies: active

## I. INTRODUCTION

In the X-ray spectra of galaxies that harbor a nuclear actively accreting, supermassive ( $10^6 \lesssim M_{\bullet}/M_{\odot} \lesssim 10^9$ ) black hole (SMBH), collectively known as Active Galactic Nuclei (AGN), the spatial origin of the fluorescent, narrow (Full Width at Half Maximum,  $\text{FWHM} < 10000 \text{ km s}^{-1}$ ) Fe K $\alpha$  emission line at a rest energy of 6.4 keV, remains elusive. This line is ubiquitous in both Type 1 and Type 2 Seyfert galaxies and AGN[1] with 2–10 keV luminosities  $< 10^{45} \text{ erg s}^{-1}$ . The line mean FWHM is  $\sim 2000 \text{ km s}^{-1}$  established from *Chandra* High Energy Transmission Grating (HETG) spectra [2–5], although [6] has suggested that the HETG line widths might actually be over-estimated. Although other, ionized Fe emission lines in the X-ray regime are also reported in AGN, all observational evidence strongly suggests that emission peaking at  $\sim 6.4$  keV is the most common Fe fluorescence feature in AGN X-ray spectra. The material in which this line arises must then be neutral and relatively cool [7, and references therein]. Because the line is narrow, it must be associated with distant matter at tens of thousands of gravitational radii from the strong-gravity regime associated with the central black hole. In this paper we are not concerned with broad Fe K $\alpha$  line emission, which may also be observed in AGN and is a manifestation of gravitational redshifting and Doppler broadening in the strong-gravity regime. All reference to “Fe K $\alpha$  emission” and “the line” will imply the narrow line.

The spatial origin of the narrow line is thus often associated with the putative obscuring, geometrically thick, dusty, molecular “torus” at a few parsecs from the SMBH. Regardless of the specific details of the torus geometry and struc-

ture, it remains an essential component of the AGN unification paradigm [8, 9, see [10–12] for reviews]. The distance from the SMBH and size can be estimated directly from the narrow-line FWHM if the BH mass is known. This allowed [4, 5] to establish that there is variation from object to object, with distances ranging from the Broad Line Region (BLR) to the Narrow Line Region (NLR) Estimates are also based on near- and mid-IR reverberation time lags [e.g. 13–17], assuming the X-ray torus is essentially the same as the IR torus. Further, although X-ray Fe K $\alpha$  reverberation is mostly associated with a *broad* Fe K $\alpha$  line [e.g. 18–22], *narrow-line* reverberation results suggest that in a prominent AGN such as NGC 4151 narrow Fe K $\alpha$  emission may originate in the inner BLR[23] [24]. In some sense the torus represents a transition region between the optical BLR closer to the nucleus and the optical NLR in the outer circumnuclear galactic environment.

Thus Fe K $\alpha$  emission origin in the BLR is also possible [e.g. 25, who report clumpy structures], but also in the region further out from the torus. It is this spatially “extended” Fe K $\alpha$  line emission that we are concerned with in this paper, as opposed to the usual  $\sim$ pc-scale narrow Fe K $\alpha$  emission closer to the nucleus. Molecular, geometrically thick obscuring material in this region beyond the torus is reported e.g. by [26] at  $\sim 30$  pc, while [27] [see also 28, 29] consider whether kpc-scale dust filaments might be sufficient to account for all obscuration. Notably, extended, specifically Fe K $\alpha$  emission, has been reported in a few nearby AGN, in which the size scale could be spatially resolved via *Chandra* CCD-imaging observations. These are usually systems estimated to be “Compton thick,” i.e. with equivalent neutral hydrogen column densities  $N_{\text{H}} \gtrsim 1.25 \times 10^{24} \text{ cm}^{-2}$ , where the

Thomson optical depth becomes  $>1$ . The flux of this extended line is usually much lower than that of the usual line associated with the torus, and as low as just a few percent of the total Fe  $K\alpha$  emission associated with a given object. In order of increasing distance from the nucleus, such emission is reported to originate up to  $\sim$ tens of pc for Circinus [30], hundreds of pc for NGC 4945 [31, 32],  $\sim 300$  pc for Mrk 3 [33][34],  $\sim 1$  kpc for ESO 428–G014 [35], and  $\sim 2.2$  kpc for NGC 1068 [36, 37]. Further, in NGC 5643 [38] an elongated north-south Fe  $K\alpha$  emission feature is identified over  $\sim 65$  pc [38]. In the case of NGC 4388, thought to be a ‘‘Compton-thin’’ AGN [39], [40] stack *Chandra* ACIS-S data from two observations and obtain significant detections of extended Fe  $K\alpha$  emission out to  $\sim 0.8$  kpc or  $\sim 10$  arcsec, most prominent in three regions, labeled ‘‘cones.’’ They use the disk-reflection continuum model of [41] with a Gaussian emission line to measure  $EW_{FeK\alpha}$  values of  $474_{-70}^{+71}$  eV and  $1.415_{-0.33}^{+0.33}$  keV, for the nucleus and the extended region, respectively. In addition, these authors compile a sample of six AGN from the literature with spatially resolved Fe  $K\alpha$  extended emission and measured equivalent widths,  $EW_{FeK\alpha}$ , which provides an extended emission  $EW_{FeK\alpha}$  baseline for comparative studies. The measured  $EW_{FeK\alpha}$  values all fall in the  $\sim 1$ -2 keV range.

These consistently large  $EW_{FeK\alpha}$  values provide the motivation for this paper, in which we use an analytical approximation to show that these observed large  $EW_{FeK\alpha}$  values are to be expected in extended AGN regions, regardless of the column density of the extended region, even when the material is Compton-thin. We use Monte Carlo (MC) simulations to calculate the extended region  $EW_{FeK\alpha}$  values for a wide range of column densities, and intrinsic continuum slopes, and show that the analytical approximation is useful for column densities up to several factors of  $10^{23}$   $\text{cm}^{-2}$ , a regime in which line-emitting matter is optically-thin to scattering or absorption at 6.4 keV.

The structure of the paper is as follows: Sec. II introduces the analytical approximation (IIA) and presents the results of MC simulations (IIB). Sec. III compares our results with published results from *Chandra* observations. We discuss our findings in Sec. IV and conclude with Sec. V which includes an overall summary.

## II. THE FE $K\alpha$ EMISSION LINE EW IN THE OPTICALLY-THIN LIMIT

### A. Analytical Calculation

We detail below how the Fe  $K\alpha$  emission line equivalent width,  $EW_{FeK\alpha}$ , can be obtained *analytically* in the optically-thin limit. This discussion is based on the very definition of equivalent width, which is given by the line flux normalized by a continuum at the line peak energy. The choice of continuum is usually what the observer measures, which may consist of contributions from more than one physically distinct regions in the source, if it is not spatially resolved. Alternatively, EW values may be calculated with respect to different continuum components obtained from modeling the net spec-

trum.

### 1. Fe $K\alpha$ line flux

Following [42], we assume a uniform, spherical distribution for the reprocessing material, with an X-ray point source located at the center, and an incident power-law continuum  $N_p E^{-\Gamma}$  photons  $\text{cm}^{-2} \text{s}^{-1}$ . The line flux is proportional to the number of continuum photons above the Fe K edge threshold,  $E_K \equiv 7.11$  keV for Fe I, that are removed, or

$$I_{FeK\alpha} = f_c \omega_K f_{K\alpha} \int_{E_K}^{\infty} N_p E^{-\Gamma} [1 - \exp(-\sigma_{FeK} A_{Fe} N_H)] dE \quad \text{photons cm}^{-2} \text{s}^{-1}, \quad (1)$$

where  $f_c \equiv \Delta\Omega/4\pi$  is the covering factor,  $\omega_K$  the fluorescence yield for neutral Fe,  $f_{K\alpha}$  the fraction of emission-line photons appearing in the Fe  $K\alpha$ , and not the Fe  $K\beta$ , line,  $\sigma_{FeK}(E)$  is the K-shell photoelectric absorption cross-section, and  $A_{Fe}$  is the Fe abundance relative to hydrogen.

We set  $\sigma_{FeK}(E) \equiv \sigma_0 (E/E_K)^{-\alpha}$ . We use  $\alpha = 2.67$  and  $\sigma_0 = 3.37 \times 10^{-20} \text{cm}^{-2}$  from fits to Verner tables [see also 43].

It is important to note that in Equation 1 line photons, once created, do not further interact with the reprocessing matter either by absorption or scattering. In other words, the reprocessor is optically-thin ( $\tau \ll 1$ ) to scattering and absorption at 6.4 keV. To linearly expand the exponential, we also impose optically thin conditions for the material to Fe-K absorption just above the Fe K edge, and thus also to all higher energies, since absorption opacity decreases with energy. In short, the optically-thin condition, both to scattering and absorption, leads to photons interacting with the material *at most once* for all energies higher than 6.4 keV.

By expanding the exponential, we then obtain the approximate relation

$$I_{FeK\alpha} \simeq f_c \omega_K f_{K\alpha} N_H A_{Fe} \sigma_0 E_K^\alpha N_p \int_{E_K}^{\infty} E^{-(\Gamma+\alpha)} dE \quad \text{photons cm}^{-2} \text{s}^{-1}. \quad (2)$$

### 2. Fe $K\alpha$ line-normalizing continuum

In general, there are two main components to the continuum emission: The direct, unscattered continuum, consisting of source photons that are neither scattered nor absorbed; and the scattered continuum. However, studies that report extended Fe  $K\alpha$  emission exclude by design emission from the AGN nucleus, and there is no other direct hard X-ray emission from the extended region. Only the scattered continuum is then of relevance for our purposes. The normalizing continuum, due to photons scattered into the line-of-sight by material with a Thomson depth  $\tau_{sc}$ , is thus given by

$$\begin{aligned} I_{sc} &= f_c N_p E_0^{-\Gamma} (1 - e^{-\tau_{sc}}) \\ &\simeq f_c N_p E_0^{-\Gamma} \tau_{sc} \\ &\simeq f_c N_p E_0^{-\Gamma} N_e N_H \sigma_T \\ &\quad \text{photons cm}^{-2} \text{s}^{-1} \text{keV}^{-1}, \end{aligned} \quad (3)$$

where  $E_0 = 6.4008$  keV, the weighted average energy of the centroids of the Fe  $K\alpha_1$  and  $K\alpha_2$  emission lines.  $N_e$  is the number of electrons per hydrogen atom. The energy is low enough that the scattering cross-section is essentially the Thomson one,  $\sigma_T$ , and the medium is optically thin to scattering ( $\tau_{sc} \ll 1$ ). As in the previous section, the optically-thin limit implies that after the first scattering a continuum photon never interacts with the medium again, i.e. the photon escape probability is essentially unity because the medium is optically thin to scattering and absorption at 6.4 keV.

It is worth pointing out that, since at lower energies the absorption opacity increases substantially, at some critical energy below 6.4 keV for a given  $N_H$ , the medium will no longer be in the optically-thin limit, and one would see absorption imprints on the scattered continuum. However, this does not affect our calculations and results, which do not involve these lower energies. Observationally, the scattered continuum may indeed show absorption signatures at low energies, and these could potentially be utilized to constrain modeling, provided the features are not too weak or swamped by other spectral features in the soft X-ray band.

### 3. Fe $K\alpha$ EW

We finally obtain an expression for the EW of the Fe  $K\alpha$  line by dividing Equation 2 by Equation 3:

$$\begin{aligned} EW_{\text{Fe}K\alpha} &= \omega_K f_{K\alpha} N_e A_{\text{Fe}} \sigma_0 \sigma_T E_K^\alpha E_0^\Gamma \int_{E_K}^{\infty} E^{-(\Gamma+\alpha)} dE \\ &\quad \text{keV} \\ &\simeq 0.970 \text{ keV} \frac{\omega_K}{0.347} \frac{f_{K\alpha}}{0.881} \frac{A_{\text{Fe}}}{4.68 \times 10^{-5}} \frac{\sigma_0}{3.368 \times 10^{-20}} \quad (4) \\ &\quad \frac{3.57}{\Gamma + \alpha - 1} (0.8985)^{(\Gamma-1.9)} \quad (5) \end{aligned}$$

We have assumed standard values for normalizing the constants in this expression [see 42]. In addition, if the hydrogen and helium abundances are  $A_H$  and  $A_{\text{He}}$ , respectively, the number of electrons per hydrogen atom is given by  $N_e = (A_H + 2A_{\text{He}})/A_H \simeq 1.22$  for the [44] abundances. While we do not assume a particular iron abundance, the value  $4.68 \times 10^{-5}$  in the equation is the [44] value for solar Fe abundance.

This result, following directly from the imposed optically-thin limit, has a remarkable implication: The EW is independent of the covering factor and column density, with the implication that the EW is also independent of the detailed geometry, even though a spherical geometry was initially assumed.

### B. Monte Carlo Simulations

We now investigate the same question, namely the magnitude of  $EW_{\text{Fe}K\alpha}$  for pure reflection as a function of  $N_H$ , by adopting a numerical approach. We show that results from Monte Carlo (MC) simulations of AGN X-ray reprocessing

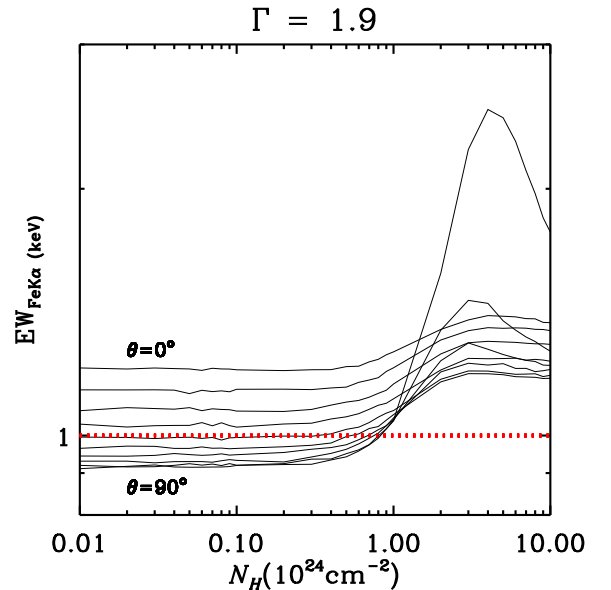


FIG. 1.  $EW_{\text{Fe}K\alpha}$  as a function of  $N_H$  in MYTORUS simulations. Different curves correspond to different  $\cos\theta$  values (or angle bins). The red horizontal line shows the analytical result for the optically-thin limit (see text). Note that this is closest to the result for angle bin 5 ( $\cos\theta = 0.5$ ), which corresponds to grazing incidence on the torus. Results are largely independent of  $N_H$  in the optically-thin and Compton-thin regime.

are entirely consistent with the above analytic approximation, but in addition extend the analytic result closer to the Compton-thick regime.

Specifically, we probe the parameter space defined by  $EW_{\text{Fe}K\alpha}$ ,  $N_H$ , intrinsic power law continuum index,  $\Gamma$ , and the cosine of the angle between the torus symmetry axis and the observer,  $\cos\theta$ . To this end, we use the MC results of ray-tracing simulations that were performed to construct the model tables now incorporated in the MYTORUS model for X-ray spectral fitting. Since we are interested in pure reflection, the direct continuum is irrelevant for this analysis.

We make use of the original MC simulations for the MYTORUS model, which are described in detail in [43] [see also 45]. Briefly, these are simulations of Green's functions, covering  $N_H$  values across the Thomson-thin to Compton-thick regime, for incident photon energies up to 500 keV, and solar Fe abundance. The reprocessed (“reflected”) continuum and its associated Fe  $K\alpha/\beta$  and Ni  $K\alpha$  emission are generated self-consistently with no ad hoc components. Using the simulation output grid, we calculate  $EW_{\text{Fe}K\alpha}$ , i.e. the equivalent width for the 0<sup>th</sup> order Fe  $K\alpha$  fluorescent line (or more precisely the weighted centroid of Fe  $K\alpha_1$  and Fe  $K\alpha_2$ ) relative to the Compton scattered continuum as a function of:

1. the cosines of the centers of 10 angle bins,  $\cos\theta_{\text{obs}}$ , corresponding to line-of-sight angles from  $\theta_{\text{obs}} = 0^\circ$  (bin 1) to  $90^\circ$  (bin 10);
2. 13 values of the intrinsic incident power-law index from

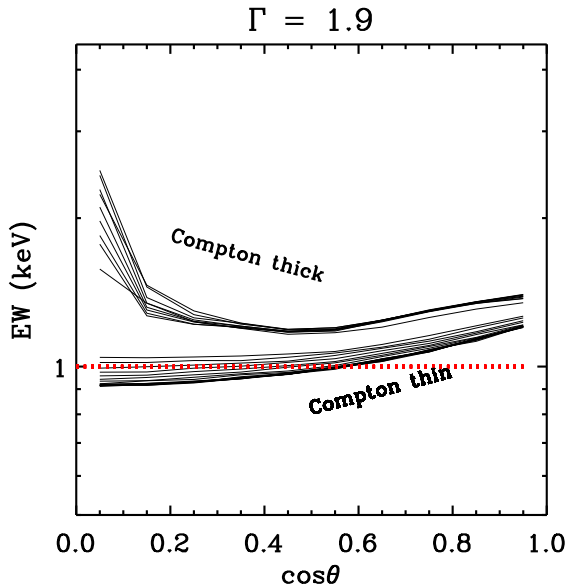


FIG. 2. Fe K $\alpha$  EW as a function of  $\cos \theta$  (or angle bin) in MYTORUS simulations. Different curves correspond to different  $N_{\text{H}}$  values in the Compton-thin (lower group of curves,  $10^{22}$  to  $10^{24}$   $\text{cm}^{-2}$ ) and Compton-thick (upper group of curves,  $2 \times 10^{24}$  to  $10^{25}$   $\text{cm}^{-2}$ ) regime. The red horizontal line shows the analytical result for the optically-thin limit (see text). Note that this is closest to the result for bin 5 ( $\cos \theta = 0.5$ ), which corresponds to grazing incidence on the torus. Results are mostly independent of  $N_{\text{H}}$  in the optically-thin and Compton-thin regimes.

$\Gamma = 1.4$  to  $2.6$ ;

- 28 values of equatorial equivalent hydrogen column density from  $N_{\text{H}} = 0.01$  to  $10$  ( $\times 10^{24} \text{cm}^{-2}$ ).

We show the simulation-based dependence of  $\text{EW}_{\text{FeK}\alpha}$  on  $N_{\text{H}}$  for  $\Gamma = 1.9$  and all angle bins in Figure 1. In a given angle bin, there appears to be no dependence on  $N_{\text{H}}$  up to  $\sim 4 \times 10^{23}$   $\text{cm}^{-2}$ . This can also be seen in Figure 2, which plots  $\text{EW}_{\text{FeK}\alpha}$  against  $\cos \theta$ . Here, there are two distinct groups of curves: The lower group corresponds to  $N_{\text{H}}$  values from  $10^{22}$  (lowest curve) to  $10^{24}$   $\text{cm}^{-2}$  (topmost curve). The upper group of curves corresponds to  $N_{\text{H}}$  values in the Compton-thick regime, from  $2 \times 10^{24}$  to  $10^{25}$   $\text{cm}^{-2}$ . In both Figures, the analytical result of the previous Section is overplotted as a dotted red line, and clearly agrees best with the MC result for bin 5 ( $\cos \theta = 0.5$ ,  $\theta = 60^\circ$ ).

It can be seen in Figure 1 that there are two extreme cases for  $\theta = 0^\circ$  and  $\theta = 90^\circ$ , effectively defining an “envelope” in  $\theta$  (and  $\cos \theta$ ). In Figure 3 we show the dependence of  $\text{EW}_{\text{FeK}\alpha}$  on  $\cos \theta$  for three characteristic  $\Gamma$  values covering a plausible range between 1.5 and 2.5. Here,  $\text{EW}_{\text{FeK}\alpha}$  is normalized by the factor  $f \equiv \frac{3.57}{\Gamma + \alpha - 1} (0.8985)^{(\Gamma - 1.9)}$  (see Equation 4), thus removing the explicit dependence on  $\Gamma$ . Note that  $f \simeq 1$  for  $\Gamma = 1.9$  (and given that  $\alpha = 2.67$ ).

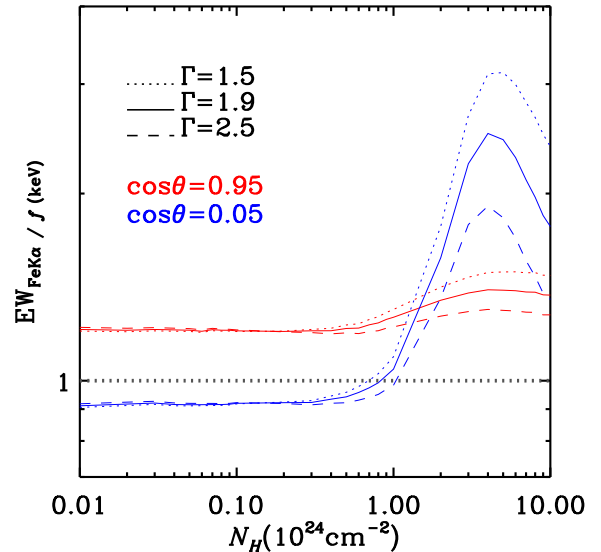


FIG. 3. Fe K $\alpha$  EW normalized by a factor  $f(\Gamma)$  (see text) as a function of  $N_{\text{H}}$  for different values of  $\cos \theta$  and  $\Gamma$ . The two extreme  $\cos \theta$  values of 0.95 (face-on, red upper curves) and 0.05 (edge-on, blue lower curves) form an envelope enclosing intermediate results (not shown for clarity). Three different  $\Gamma$  values are shown by a dotted, dashed, and solid curve in each  $\cos \theta$  case. The analytical optically-thin limit (Equation 4) is shown by the grey dotted horizontal line. Results are clearly independent of  $N_{\text{H}}$  up to  $\sim 3 - 5 \times 10^{23}$   $\text{cm}^{-2}$ , with the exact threshold of dependence slightly depending on  $\theta$  and  $\Gamma$ .

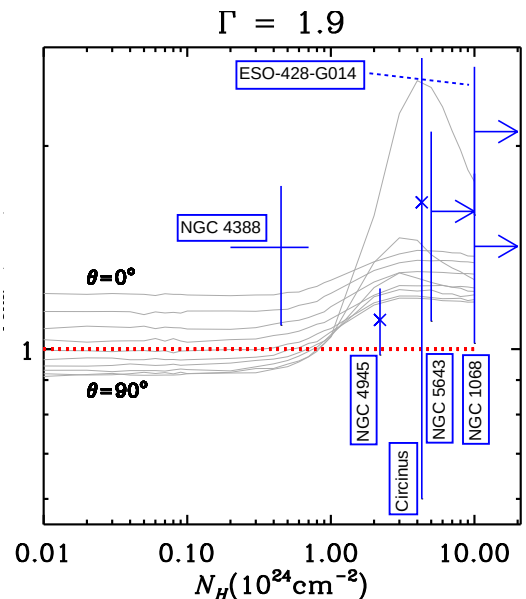


FIG. 4. Same as Figure 1 with data for the six AGN with detected Fe K $\alpha$  extended emission from the compilation of [40, Table 4] as indicated. The right-pointing arrows represent lower limits. Otherwise, blue line segments represent the range of estimated values, taking into account both ranges of measurements and reported uncertainties, where available.

### III. COMPARISON WITH CHANDRA OBSERVATIONS

Figure 4 is a modified version of Figure 1, with the *Chandra*-based compilation of results for detected extended Fe K $\alpha$  emission presented in [40, Table 4] overplotted. As explained by these authors, the reported results for Circinus cover a range of earlier results in  $EW_{\text{FeK}\alpha}$ . For clarity, we show here the full range in  $EW_{\text{FeK}\alpha}$  for this object, taking into account uncertainties. The average central value is shown with a cross. For the remaining systems, we show single  $EW_{\text{FeK}\alpha}$  central values with uncertainties from the references reported in [40]. Observationally estimated  $N_{\text{H}}$  values compiled by [40] do not have uncertainties. For NGC 4388 the horizontal “error bar” represents the range of reported  $N_{\text{H}}$  central values. Three other AGN have lower limits in  $N_{\text{H}}$  as indicated by the arrows.

Focusing on  $EW_{\text{FeK}\alpha}$  values shown in Figure 4, we note that all reported values are within a factor of  $\sim 2$  of the analytic approximation of  $\sim 1$  keV. In the case of Compton-thin NGC 4388 in particular, which is most consistent with the assumptions of the analytic approximation,  $EW_{\text{FeK}\alpha}$  is also close to the analytic value within the reported  $EW_{\text{FeK}\alpha}$  errors. Finally, all  $EW_{\text{FeK}\alpha}$  values are consistent with the MC values within the reported uncertainties and ranges.

### IV. RESULTS AND DISCUSSION

A key result from this work is that the optically-thin analytic approximation for  $EW_{\text{FeK}\alpha}$  is surprisingly close to the MC results for column densities that go well beyond the optically-thin regime, up to  $N_{\text{H}} \lesssim 4 \times 10^{23} \text{ cm}^{-2}$ . In this regime,  $EW_{\text{FeK}\alpha}$  is only weakly dependent on  $\theta$ . We discuss these results further below.

Figures 1 and 2 show that the  $EW_{\text{FeK}\alpha}$  estimated analytically is within  $\lesssim 20\%$  for *all* MC estimates, regardless of  $\theta$  bin, and up to  $N_{\text{H}} \sim 4 \times 10^{23} \text{ cm}^{-2}$ . This is highlighted in the fractional difference versions of the figures, i.e. Figures 5 and 6. For  $\theta = 60^\circ$  the agreement is within  $\sim 1\%$ , and even at  $\sim 10^{24} \text{ cm}^{-2}$  it is within  $\sim 5\%$  (red curve in Figure 5). The optically-thin analytic approximation for  $EW_{\text{FeK}\alpha}$  was derived assuming a spherical geometry, which necessarily has material intercepting the line of sight, and it aligns most closely with the MC angular bin that has the smallest non-zero column density. This is the grazing-incidence angle bin, which has its bin boundary at  $\cos \theta = 0.5$ , corresponding to  $\theta = 60^\circ$ . The analytic  $EW_{\text{FeK}\alpha}$  approximation does not agree as well with MC results for other angle bins, in particular those not intercepting any material, even for small column densities, because it assumes non-zero columns of material in the line of sight. Even so, an agreement within  $\sim 20\%$  for all bins is a significant result.

Further, Figure 3 shows that curves of  $EW_{\text{FeK}\alpha}$  as a function of  $N_{\text{H}}$  diverge for different  $\Gamma$  values above  $N_{\text{H}} \sim 4 \times 10^{23} \text{ cm}^{-2}$ , implying that the  $\Gamma$  dependence of  $EW_{\text{FeK}\alpha}$  in the analytic approximation fails to capture the physics above this column density. Thus, the analytic approximation breaks down above  $N_{\text{H}} \sim 4 \times 10^{23} \text{ cm}^{-2}$ , and this column density represents the approximate upper limit of applicability of the analytic ap-

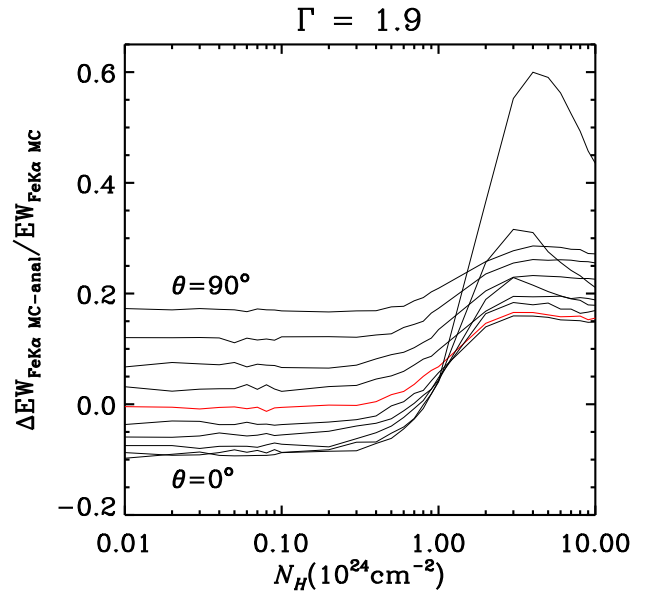


FIG. 5. As Figure 1 but for the *fractional* difference between  $EW_{\text{FeK}\alpha}$  from MC simulations compared to the optically-thin limit (analytic result in Equation 4) as a function of  $N_{\text{H}}$ . The red curve corresponds to angle bin 5 ( $\cos \theta = 0.5$ ) in the simulations.

proximation. This column density corresponds to a Thomson depth of 0.32.

One might ask whether the toroidal geometry which is assumed in the MYTORUS simulations might reduce the generality of these results. In the optically-thin regime, the agreement with the analytical approximation, which does not assume such a geometry, is one indication that this should not be an issue. In the Compton-thick regime, we note the independent MC results of [46], who assume a uniform spherical geometry, obtaining  $EW_{\text{FeK}\alpha} \gtrsim 1$  keV that increases with optical depth / column density. Even though these authors do not exclude the direct continuum in their  $EW_{\text{FeK}\alpha}$  calculations as we do, excluding the direct continuum would only further *enhance* the large  $EW_{\text{FeK}\alpha}$  effect, as we observe. Finally, even if the toroidal geometry were to have some effect, we still see that regardless of angle  $\theta$ ,  $EW_{\text{FeK}\alpha}$  remains  $> 1$  keV for all  $N_{\text{H}}$  probed. This strongly suggests that the dominant effect is the exclusion of the direct continuum.

In the case of a clumpy geometry, each clump will produce a large  $EW_{\text{FeK}\alpha}$  as, once more, this would be measured relative to the scattered continuum only. The ensemble of clumps would then give rise to an overall large  $EW_{\text{FeK}\alpha}$ . In the limit of a high-filling factor, the results would be as for a sphere, discussed above [see 46], and in the optically thin limit the analytic approximation would once again hold.

Overall, given the simple assumptions underlying the analytic approximation, and the fact that one might expect it to fail significantly above  $10^{22} \text{ cm}^{-2}$ , this is a significant result, that provides a simple explanation for large equivalent widths of Fe K $\alpha$  emission lines in extended AGN regions.

[40] note that  $EW_{\text{FeK}\alpha}$  values are  $\sim 3$  times larger in the

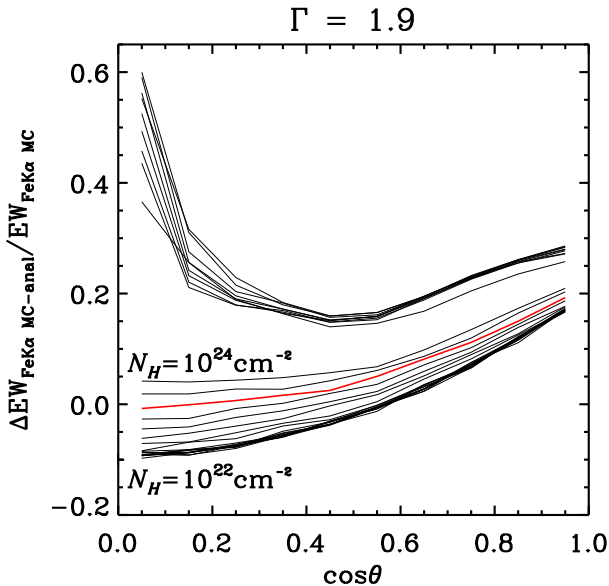


FIG. 6. As Figure 2 but for the *fractional* difference between  $EW_{\text{FeK}\alpha}$  from MC simulations compared to the analytic result (Equation 4, optically-thin limit) as a function of  $\cos \theta$ . The red curve corresponds to the MC simulation bin for  $N_{\text{H}} = 8 \times 10^{23} \text{ cm}^{-2}$ .

extended region compared to those for regions closer to the nucleus. They attribute this to differences in geometry or Fe abundance between the circumnuclear and the extended region. However, it should be pointed out that a major issue with such an explanation is that increasing the Fe abundance does not linearly increase  $EW_{\text{FeK}\alpha}$  because more Fe also means more absorption (including of line photons), and not just K- but also L-shell absorption. To increase  $EW_{\text{FeK}\alpha}$  by a factor of  $\sim 3$ , you need *at least an order of magnitude* increase in Fe abundance [see 47, Fig. 17], by which point the continuum will have become completely skewed and wrong. Further, as also explained by [40, see also references therein], an increase in iron abundance would mainly be introduced via delayed SN Ia enrichment over timescales of  $\sim 1$  Gyr, but this would be unlikely to remain preferentially in the extended circumnuclear region over such prolonged periods of time. Differences in geometry would imply that somehow more X-ray reprocessing material would be located at larger scales compared to those usually attributed to torus-like structures, which are thought to be up to few pc based on virial assumptions for the Fe K $\alpha$  line width, IR reverberation mapping, and ALMA sub-mm imaging [e.g. 4, 48–51]. [40] further consider the possibility of an intrinsically depressed AGN continuum which would naturally favor larger EW measurements. This however should also affect the EW measured for Fe K $\alpha$  emission originating closer to the central AGN.

Instead, qualitatively  $EW_{\text{FeK}\alpha}$  in the extended region would naturally be expected to be larger than that for the more common narrow Fe K $\alpha$  line arising closer to the nucleus, simply because *the extended-emission line equivalent width is measured only with respect to the scattered continuum*, which is

not the case for the more common line. This is a key point, and to our knowledge, no previous work on  $EW_{\text{FeK}\alpha}$  has appropriately taken this into account. In this paper we are highlighting and quantifying this effect both analytically and computationally. Both approaches corroborate the qualitative expectation, and are also in agreement with each other.

Both of the analytical expressions for the line flux (Equations 1 and 2), as well as the one for the normalizing scattered continuum (Equation 3), assume that the reprocessing matter is optically thin to both absorption and scattering. Line photons effectively do not interact with this matter after being created; similarly, continuum photons never interact with the medium after the first scattering (either by absorption or further scattering). Put differently, in both cases, we are setting the photon escape probability function to unity, which is justified in this regime. In general, the  $EW_{\text{FeK}\alpha}$  expression (Equation 4) should include such an escape function both in the numerator and the denominator. These functions will be different in general, but when the medium is optically thin, one can reasonably assume that the spatial distribution of line creation sites and that of scattering sites are the same because both are distributed uniformly in the medium. However, as the optical depth increases, these distributions will not remain the same, and the two escape functions become different. What we have effectively done is to use the MC results as a computational experiment to probe the evolution of these escape functions. As we have shown, the reasonable, qualitative assumption that the spatial distributions of the line creation and continuum scattering sites are similar holds up to column densities  $N_{\text{H}} \sim 4 \times 10^{23} \text{ cm}^{-2}$ . Therefore, they cancel out in the analytical  $EW_{\text{FeK}\alpha}$  expression, thus making  $EW_{\text{FeK}\alpha}$  independent of  $N_{\text{H}}$ .

As to the actual nature of the extended emission material, we note that cold, molecular material due to outflows in AGN at larger, tens to hundreds of pc, scales has also been detected in the sub-mm [52–56]. Recently, detections of molecular tori with extended diameter sizes up to  $\sim 50$  pc are reported [57, 58] extending the obscuring torus itself beyond the pc-scale paradigm. The proposed combined emerging molecular and IR picture includes both outflows and feeding inflows from resonant molecular reservoirs at  $\sim 100$  pc [51, 57, 59–63] or more. Overall, such molecular material would also be a candidate for an extended X-ray reprocessor.

It is clear that even AGN with moderate levels of obscuration, such as NGC 4388 and Mrk 3, do show extended Fe K $\alpha$  emission over spatial scales of at least hundreds of parsecs, with associated keV-scale EWs. Our MC results have shown that a large  $EW_{\text{FeK}\alpha}$  would be naturally expected *for all*  $N_{\text{H}}$ . Since NGC 4388 is Compton-thin, its large  $EW_{\text{FeK}\alpha}$  should also be better predicted by the analytic approximation (which, however, is based on the stricter optically-thin condition) and the analytical result of  $\sim 1$  keV for  $EW_{\text{FeK}\alpha}$  is in good agreement with the lower limit of the value reported by the *Chandra* analysis, i.e. 1.085 keV. The analytical result is also entirely consistent with  $EW_{\text{FeK}\alpha}$  values of 0.7–1 keV reported as due to molecular clouds around Sgr A\* scattering X-ray emission from nuclear flares [64], although these clouds are thought to be located tens rather than hundreds of parsecs away from the

nucleus.

Thus, overall, both the MC results and the analytical approximation suggest that large  $EW_{\text{FeK}\alpha}$  signatures should be ubiquitous at kpc-scale distances from AGN, and the few available observational results are in support of this picture.

## V. SUMMARY AND CONCLUSIONS

We have shown that the narrow Fe K $\alpha$  emission equivalent width observed at  $\sim$ kpc scales in AGN can be predicted both analytically and numerically, and have compared these predictions to observed results from the literature. Our main conclusions are:

1. Calculations of  $EW_{\text{FeK}\alpha}$  in the optically-thin limit, coupled with the absence of the direct X-ray AGN continuum from the extended region, lead to an analytic approximate estimate  $EW_{\text{FeK}\alpha,\text{approx}} \sim 1$  keV that is independent of  $N_{\text{H}}$  or geometric details such as covering factor.
2. Using state-of-the-art MC ray-tracing simulations with MYTORUS, we show that  $EW_{\text{FeK}\alpha,\text{MC}}$ :
  - (a) is independent of  $N_{\text{H}}$  up to  $\sim 4 \times 10^{23} \text{ cm}^{-2}$ ;
  - (b) is mildly dependent on the angle to the line-of-sight,  $\theta$ , and the power law index,  $\Gamma$ ;
  - (c) is within  $\sim 20\%$  ( $\sim 1\%$ ) of  $EW_{\text{FeK}\alpha,\text{approx}}$  for all  $\theta$  (for  $\theta = 60^\circ$ ) up to  $\sim 4 \times 10^{23} \text{ cm}^{-2}$ ;
  - (d) is consistently  $> 1$  keV as the  $N_{\text{H}}$  increases into the Compton-thick  $N_{\text{H}}$  regime, suggesting that large  $EW_{\text{FeK}\alpha}$  values are to be expected for all  $N_{\text{H}}$ .
3. We argue that these results should remain unaffected by toroidal, spherical, or clumpy geometries. However,

the results do not carry over to the absolute flux of the Fe K $\alpha$  line (as opposed to the EW): [65] showed that for line flux, the optically-thin approximation breaks down at a column density of only  $\sim 4 \times 10^{22} \text{ cm}^{-2}$ .

4. Both  $EW_{\text{FeK}\alpha,\text{MC}}$  and  $EW_{\text{FeK}\alpha,\text{approx}}$  are within a factor of  $\sim 2$  from observational estimates for  $EW_{\text{FeK}\alpha}$  at  $\sim$ kpc scales in local AGN.

The  $EW_{\text{FeK}\alpha,\text{MC}}$  and  $EW_{\text{FeK}\alpha,\text{approx}}$  good agreement up to  $N_{\text{H}} \sim 4 \times 10^{23} \text{ cm}^{-2}$  directly demonstrates and quantifies a reasonable expectation in the optically-thin regime. Beyond this, the MC results show that  $EW_{\text{FeK}\alpha}$  will remain larger than 1 keV into the Compton-thick regime, a prediction that should be tested further with more observational data. This agreement, as well as the order-of-magnitude agreement with observational results, suggest that the relative prevalence of narrow Fe K $\alpha$  AGN emission at kpc scales beyond the ‘‘canonical’’ torus follows a roughly predictable pattern across AGN and at least two orders of magnitude in  $N_{\text{H}}$ . Larger AGN samples with such detections, as well as multiwavelength detections in the IR and sub-mm, would provide further insight into the nature and frequency of large-scale X-ray AGN reflection. It also remains to be explored whether similar  $EW_{\text{FeK}\alpha}$  behavior can be established at the smaller spatial scales of Galactic X-ray binaries.

## ACKNOWLEDGMENTS

We thank the anonymous referee for their constructive comments that helped improve this paper. P.T. acknowledges support from NASA grants 80NSSC18K0408 (solicitation NNH17ZDA001N-ADAP) and 80NSSC22K0411 (solicitation NNH21ZDA001N-ADAP). This work is supported by NASA under the CRESST Cooperative Agreement, award number 80GSFC21M0002.

- 
- [1] We use these terms interchangeably in this paper.
  - [2] T. Yaqoob and U. Padmanabhan, *ApJ* **604**, 63 (2004), [astro-ph/0311551](#).
  - [3] K. Nandra, *MNRAS* **368**, L62 (2006), [astro-ph/0602081](#).
  - [4] X. W. Shu, T. Yaqoob, and J. X. Wang, *ApJS* **187**, 581 (2010), [arXiv:1003.1790 \[astro-ph.HE\]](#).
  - [5] X. W. Shu, T. Yaqoob, and J. X. Wang, *ApJ* **738**, 147 (2011), [arXiv:1107.0195](#).
  - [6] J. Liu, *MNRAS* **463**, L108 (2016), [arXiv:1608.07351 \[astro-ph.HE\]](#).
  - [7] G. Ghisellini, F. Haardt, and G. Matt, *MNRAS* **267**, 743 (1994), [arXiv:astro-ph/9401044 \[astro-ph\]](#).
  - [8] R. Antonucci, *ARA&A* **31**, 473 (1993).
  - [9] C. M. Urry and P. Padovani, *PASP* **107**, 803 (1995), [astro-ph/9506063](#).
  - [10] H. Netzer, *ARA&A* **53**, 365 (2015), [arXiv:1505.00811](#).
  - [11] R. C. Hickox and D. M. Alexander, *ARA&A* **56**, 625 (2018), [arXiv:1806.04680 \[astro-ph.GA\]](#).
  - [12] P. Padovani, D. M. Alexander, R. J. Assef, B. De Marco, P. Giommi, R. C. Hickox, G. T. Richards, V. Smolčić, E. Hatziminaoglou, V. Mainieri, and M. Salvato, *A&A Rv* **25**, 2 (2017), [arXiv:1707.07134 \[astro-ph.GA\]](#).
  - [13] L. Burtscher, K. Meisenheimer, K. R. W. Tristram, W. Jaffe, S. F. Hönig, R. I. Davies, M. Kishimoto, J. U. Pott, H. Röttgering, M. Schartmann, G. Weigelt, and S. Wolf, *A&A* **558**, A149 (2013), [arXiv:1307.2068 \[astro-ph.CO\]](#).
  - [14] F. Pozo Nuñez, M. Ramolla, C. Westhues, M. Haas, R. Chini, K. Steenbrugge, A. Barr Domínguez, L. Kaderhandt, M. Hackstein, W. Kollatschny, M. Zetzl, K. W. Hodapp, and M. Murphy, *A&A* **576**, A73 (2015), [arXiv:1502.06771 \[astro-ph.GA\]](#).
  - [15] T. Almeyda, A. Robinson, M. Richmond, R. Nikutta, and B. McDonough, *ApJ* **891**, 26 (2020), [arXiv:2002.12823 \[astro-ph.GA\]](#).
  - [16] C. Sobrino Figaredo, M. Haas, M. Ramolla, R. Chini, J. Blex, K. W. Hodapp, M. Murphy, W. Kollatschny, D. Chelouche, and S. Kaspi, *AJ* **159**, 259 (2020), [arXiv:2004.10244 \[astro-ph.GA\]](#).
  - [17] J. Lyu and G. H. Rieke, *ApJ* **912**, 126 (2021), [arXiv:2011.07638 \[astro-ph.GA\]](#).
  - [18] A. C. Fabian, A. Zoghbi, R. R. Ross, P. Uttley, L. C. Gallo, W. N. Brandt, A. J. Blustin, T. Boller, M. D. Caballero-Garcia, J. Larsson, J. M. Miller, G. Miniutti, G. Ponti, R. C. Reis, C. S. Reynolds, Y. Tanaka, and A. J. Young, *Nature* **459**, 540 (2009).
  - [19] A. Zoghbi, A. C. Fabian, P. Uttley, G. Miniutti, L. C. Gallo, C. S. Reynolds, J. M. Miller, and G. Ponti, *MNRAS* **401**, 2419

- (2010), [arXiv:0910.0367 \[astro-ph.HE\]](#).
- [20] A. Zoghbi, C. Reynolds, E. M. Cackett, G. Miniutti, E. Kara, and A. C. Fabian, *ApJ* **767**, 121 (2013), [arXiv:1302.1761 \[astro-ph.HE\]](#).
- [21] E. Kara, W. N. Alston, A. C. Fabian, E. M. Cackett, P. Uttley, C. S. Reynolds, and A. Zoghbi, *MNRAS* **462**, 511 (2016), [arXiv:1605.02631 \[astro-ph.HE\]](#).
- [22] E. M. Cackett, M. C. Bentz, and E. Kara, *iScience* **24**, 102557 (2021), [arXiv:2105.06926 \[astro-ph.GA\]](#).
- [23] This object was formerly also a famous candidate for *relativistic* Fe  $K\alpha$  reverberation, but this is no longer the case; see [24].
- [24] A. Zoghbi, J. M. Miller, and E. Cackett, *ApJ* **884**, 26 (2019), [arXiv:1908.09862 \[astro-ph.HE\]](#).
- [25] J.-M. Wang, P. Du, M. S. Brotherton, C. Hu, Y.-Y. Songsheng, Y.-R. Li, Y. Shi, and Z.-X. Zhang, *Nature Astronomy* **1**, 775 (2017), [arXiv:1710.03419 \[astro-ph.GA\]](#).
- [26] E. K. S. Hicks, R. I. Davies, M. A. Malkan, R. Genzel, L. J. Tacconi, F. Müller Sánchez, and A. Sternberg, *ApJ* **696**, 448 (2009), [arXiv:0902.0978 \[astro-ph.GA\]](#).
- [27] M. A. Prieto, M. Mezcuca, J. A. Fernández-Ontiveros, and M. Schartmann, *MNRAS* **442**, 2145 (2014), [arXiv:1405.5653 \[astro-ph.GA\]](#).
- [28] A. D. Goulding and D. M. Alexander, *MNRAS* **398**, 1165 (2009), [arXiv:0906.0772 \[astro-ph.CO\]](#).
- [29] A. D. Goulding, D. M. Alexander, F. E. Bauer, W. R. Forman, R. C. Hickox, C. Jones, J. R. Mullaney, and M. Trichas, *ApJ* **755**, 5 (2012), [arXiv:1205.1800 \[astro-ph.GA\]](#).
- [30] A. Marinucci, G. Miniutti, S. Bianchi, G. Matt, and G. Risaliti, *MNRAS* **436**, 2500 (2013), [arXiv:1309.4456 \[astro-ph.CO\]](#).
- [31] A. Marinucci, G. Risaliti, J. Wang, E. Nardini, M. Elvis, G. Fabbiano, S. Bianchi, and G. Matt, *MNRAS* **423**, L6 (2012), [arXiv:1202.1279 \[astro-ph.CO\]](#).
- [32] A. Marinucci, S. Bianchi, G. Fabbiano, G. Matt, G. Risaliti, E. Nardini, and J. Wang, *MNRAS* **470**, 4039 (2017), [arXiv:1706.06362 \[astro-ph.HE\]](#).
- [33] M. Guainazzi, V. La Parola, G. Miniutti, A. Segreto, and A. L. Longinotti, *A&A* **547**, A31 (2012), [arXiv:1209.0706 \[astro-ph.CO\]](#).
- [34] [66] report a column density in the Compton-thin regime.
- [35] G. Fabbiano, M. Elvis, A. Paggi, M. Karovska, W. P. Maksym, J. Raymond, G. Risaliti, and J. Wang, *ApJL* **842**, L4 (2017), [arXiv:1705.10680 \[astro-ph.HE\]](#).
- [36] A. J. Young, A. S. Wilson, and P. L. Shopbell, *ApJ* **556**, 6 (2001), [arXiv:astro-ph/0104027 \[astro-ph\]](#).
- [37] F. E. Bauer, P. Arévalo, D. J. Walton, M. J. Koss, S. Puccetti, P. Gandhi, D. Stern, D. M. Alexander, M. Baloković, S. E. Boggs, W. N. Brandt, M. Brightman, F. E. Christensen, A. Comastri, W. W. Craig, A. Del Moro, C. J. Hailey, F. A. Harrison, R. Hickox, B. Luo, C. B. Markwardt, A. Marinucci, G. Matt, J. R. Rigby, E. Rivers, C. Saez, E. Treister, C. M. Urry, and W. W. Zhang, *ApJ* **812**, 116 (2015), [arXiv:1411.0670 \[astro-ph.HE\]](#).
- [38] G. Fabbiano, A. Paggi, A. Siemiginowska, and M. Elvis, *ApJL* **869**, L36 (2018), [arXiv:1812.02764 \[astro-ph.HE\]](#).
- [39] T. Yaqoob, P. Tzanavaris, and S. LaMassa, *MNRAS* **522**, 394 (2023).
- [40] H. Yi, J. Wang, X. Shu, G. Fabbiano, C. Pappalardo, C. Wang, and H. Yu, *ApJ* **908**, 156 (2021), [arXiv:2012.04900 \[astro-ph.GA\]](#).
- [41] P. Magdziarz and A. A. Zdziarski, *MNRAS* **273**, 837 (1995).
- [42] T. Yaqoob, I. M. George, K. Nandra, T. J. Turner, P. J. Serlemitsos, and R. F. Mushotzky, *ApJ* **546**, 759 (2001), [astro-ph/0008471](#).
- [43] K. D. Murphy and T. Yaqoob, *MNRAS* **397**, 1549 (2009), [arXiv:0905.3188 \[astro-ph.HE\]](#).
- [44] E. Anders and N. Grevesse, *GeCoA* **53**, 197 (1989).
- [45] T. Yaqoob, *MNRAS* **423**, 3360 (2012), [arXiv:1204.4196 \[astro-ph.HE\]](#).
- [46] D. A. Leahy and J. Creighton, *MNRAS* **263**, 314 (1993).
- [47] I. M. George and A. C. Fabian, *MNRAS* **249**, 352 (1991).
- [48] P. Gandhi, S. F. Hönic, and M. Kishimoto, *ApJ* **812**, 113 (2015), [arXiv:1502.02661 \[astro-ph.HE\]](#).
- [49] S. García-Burillo, F. Combes, C. Ramos Almeida, A. Usero, M. Krips, A. Alonso-Herrero, S. Aalto, V. Casasola, L. K. Hunt, S. Martín, S. Viti, L. Colina, F. Costagliola, A. Eckart, A. Fuente, C. Henkel, I. Márquez, R. Neri, E. Schinnerer, L. J. Tacconi, and P. P. van der Werf, *ApJL* **823**, L12 (2016), [arXiv:1604.00205 \[astro-ph.GA\]](#).
- [50] S. García-Burillo, F. Combes, C. Ramos Almeida, A. Usero, A. Alonso-Herrero, L. K. Hunt, D. Rouan, S. Aalto, M. Querejeta, S. Viti, P. P. van der Werf, H. Vives-Arias, A. Fuente, L. Colina, J. Martín-Pintado, C. Henkel, S. Martín, M. Krips, D. Gratadour, R. Neri, and L. J. Tacconi, *A&A* **632**, A61 (2019), [arXiv:1909.00675 \[astro-ph.GA\]](#).
- [51] S. F. Hönic, *ApJ* **884**, 171 (2019), [arXiv:1909.08639 \[astro-ph.GA\]](#).
- [52] S. J. Curran, B. S. Koribalski, and I. Bains, *MNRAS* **389**, 63 (2008), [arXiv:0807.4766 \[astro-ph\]](#).
- [53] L. K. Zschaechner, F. Walter, A. Bolatto, E. P. Farina, J. M. D. Kruijssen, A. Leroy, D. S. Meier, J. Ott, and S. Veilleux, *ApJ* **832**, 142 (2016), [arXiv:1609.06316 \[astro-ph.GA\]](#).
- [54] J. F. Gallimore, M. Elitzur, R. Maiolino, A. Marconi, C. P. O’Dea, D. Lutz, S. A. Baum, R. Nikutta, C. M. V. Impellizzeri, R. Davies, A. E. Kimball, and E. Sani, *ApJL* **829**, L7 (2016), [arXiv:1608.02210 \[astro-ph.GA\]](#).
- [55] K. Alatalo, L. Blitz, L. M. Young, T. A. Davis, M. Bureau, L. A. Lopez, M. Cappellari, N. Scott, K. L. Shapiro, A. F. Crocker, S. Martín, M. Bois, F. Bournaud, R. L. Davies, P. T. de Zeeuw, P. A. Duc, E. Emsellem, J. Falcón-Barroso, S. Khochfar, D. Krajnović, H. Kuntschner, P. Y. Lablanche, R. M. McDermid, R. Morganti, T. Naab, T. Oosterloo, M. Sarzi, P. Serra, and A. Weijmans, *ApJ* **735**, 88 (2011), [arXiv:1104.2326 \[astro-ph.CO\]](#).
- [56] A. D. Bolatto, A. K. Leroy, R. C. Levy, D. S. Meier, E. A. C. Mills, T. A. Thompson, K. L. Emig, S. Veilleux, J. Ott, M. Gorski, F. Walter, L. A. Lopez, and L. Lenkić, *ApJ* **923**, 83 (2021), [arXiv:2109.10437 \[astro-ph.GA\]](#).
- [57] F. Combes, S. García-Burillo, A. Audibert, L. Hunt, A. Eckart, S. Aalto, V. Casasola, F. Boone, M. Krips, S. Viti, K. Sakamoto, S. Muller, K. Dasyra, P. van der Werf, and S. Martin, *A&A* **623**, A79 (2019), [arXiv:1811.00984 \[astro-ph.GA\]](#).
- [58] S. García-Burillo, A. Alonso-Herrero, C. Ramos Almeida, O. González-Martín, F. Combes, A. Usero, S. Hönic, M. Querejeta, E. K. S. Hicks, L. K. Hunt, D. Rosario, R. Davies, P. G. Boorman, A. J. Bunker, L. Burtscher, L. Colina, T. Díaz-Santos, P. Gandhi, I. García-Bernete, B. García-Lorenzo, K. Ichikawa, M. Imanishi, T. Izumi, A. Labiano, N. A. Levenson, E. López-Rodríguez, C. Packham, M. Pereira-Santaella, C. Ricci, D. Rigopoulou, D. Rouan, T. Shimizu, M. Stalevski, K. Wada, and D. Williamson, *A&A* **652**, A98 (2021), [arXiv:2104.10227 \[astro-ph.GA\]](#).
- [59] C. Ramos Almeida and C. Ricci, *Nature Astronomy* **1**, 679 (2017), [arXiv:1709.00019 \[astro-ph.GA\]](#).
- [60] A. Alonso-Herrero, M. Pereira-Santaella, S. García-Burillo, R. I. Davies, F. Combes, D. Asmus, A. Bunker, T. Díaz-Santos, P. Gandhi, O. González-Martín, A. Hernán-Caballero, E. Hicks, S. Hönic, A. Labiano, N. A. Levenson, C. Packham, C. Ramos Almeida, C. Ricci, D. Rigopoulou, D. Rosario, E. Sani, and



- M. J. Ward, *ApJ* **859**, 144 (2018), [arXiv:1804.04842 \[astro-ph.GA\]](#).
- [61] T. Izumi, K. Wada, R. Fukushige, S. Hamamura, and K. Kohno, *ApJ* **867**, 48 (2018), [arXiv:1809.09154 \[astro-ph.GA\]](#).
- [62] A. Alonso-Herrero, S. García-Burillo, M. Pereira-Santaella, R. I. Davies, F. Combes, M. Vestergaard, S. I. Raimundo, A. Bunker, T. Díaz-Santos, P. Gandhi, I. García-Berete, E. K. S. Hicks, S. F. Hönic, L. K. Hunt, M. Imanishi, T. Izumi, N. A. Levenson, W. Maciejewski, C. Packham, C. Ramos Almeida, C. Ricci, D. Rigopoulou, P. F. Roche, D. Rosario, M. Schartmann, A. Usero, and M. J. Ward, *A&A* **628**, A65 (2019), [arXiv:1906.06889 \[astro-ph.GA\]](#).
- [63] A. Alonso-Herrero, S. García-Burillo, S. F. Hönic, I. García-Berete, C. Ramos Almeida, O. González-Martín, E. López-Rodríguez, P. G. Boorman, A. J. Bunker, L. Burtscher, F. Combes, R. Davies, T. Díaz-Santos, P. Gandhi, B. García-Lorenzo, E. K. S. Hicks, L. K. Hunt, K. Ichikawa, M. Imanishi, T. Izumi, A. Labiano, N. A. Levenson, C. Packham, M. Pereira-Santaella, C. Ricci, D. Rigopoulou, P. Roche, D. J. Rosario, D. Rouan, T. Shimizu, M. Stalevski, K. Wada, and D. Williamson, *A&A* **652**, A99 (2021), [arXiv:2107.00244 \[astro-ph.GA\]](#).
- [64] G. Ponti, R. Terrier, A. Goldwurm, G. Belanger, and G. Trap, *ApJ* **714**, 732 (2010), [arXiv:1003.2001 \[astro-ph.HE\]](#).
- [65] T. Yaqoob, K. D. Murphy, L. Miller, and T. J. Turner, *MNRAS* **401**, 411 (2010), [arXiv:0909.0899 \[astro-ph.HE\]](#).
- [66] M. Guainazzi, G. Risaliti, H. Awaki, P. Arevalo, F. E. Bauer, S. Bianchi, S. E. Boggs, W. N. Brandt, M. Brightman, F. E. Christensen, W. W. Craig, K. Forster, C. J. Hailey, F. Harrison, M. Koss, A. Longinotti, C. Markwardt, A. Marinucci, G. Matt, C. S. Reynolds, C. Ricci, D. Stern, J. Svoboda, D. Walton, and W. Zhang, *MNRAS* **460**, 1954 (2016), [arXiv:1605.02467 \[astro-ph.HE\]](#).